JACS
JOURNAL OF THE AMERICAN CHEMICAL SOCIETY

Intramolecular Light-Driven Accumulation of Reduction Equivalents by Proton-Coupled Electron Transfer
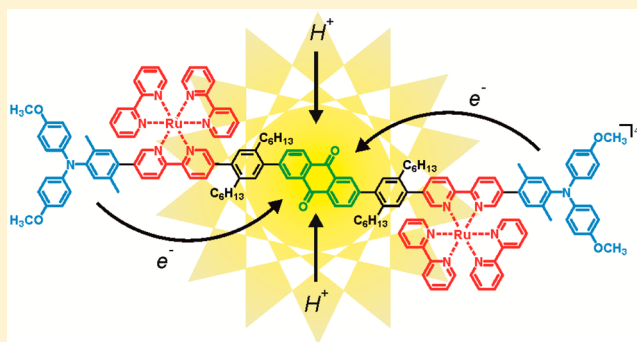
Martin Kuss-Petermann,[†,‡] Margherita Orazietti,[¶,‡] Markus Neuburger,[†] Peter Hamm,*,[¶] and Oliver S. Wenger*,[†]

[†]Department of Chemistry, University of Basel, St. Johanns-Ring 19, 4056 Basel, Switzerland
[¶]Department of Chemistry, University of Zurich, Winterthurerstrasse 190, 8057 Zurich, Switzerland

S Supporting Information

ABSTRACT: The photochemistry of a molecular pentad composed of a central anthraquinone (AQ) acceptor flanked by two $Ru(bpy)_3^{2+}$ photosensitizers and two peripheral triarylamine (TAA) donors was investigated by transient IR and UV−vis spectroscopies in the presence of 0.2 M p-toluenesulfonic acid (TsOH) in deaerated acetonitrile. In ∼15% of all excited pentad molecules, AQ is converted to its hydroquinone form (AQH_2) via reversible intramolecular electron transfer from the two TAA units (τ = 65 ps), followed by intermolecular proton transfer from TsOH ($\tau \approx 3$ ns for the first step). Although the light-driven accumulation of reduction equivalents occurs through a sequence of electron and proton transfer steps, the resulting photoproduct decays via concerted PCET (τ = 4.7 μs) with an H/D kinetic isotope effect of 1.4 ± 0.2. Moreover, the reoxidation of AQH_2 seems to take place via a double electron transfer step involving both TAA$^+$ units rather than sequential single electron transfer events. Thus, the overall charge-recombination reaction seems to involve a concerted proton-coupled two-electron oxidation of AQH_2. The comparison of experimental data obtained in neat acetonitrile with data from acidic solutions suggests that the inverted driving-force effect can play a crucial role for obtaining long-lived photoproducts resulting from multiphoton, multielectron processes. Our pentad provides the first example of light-driven accumulation of reduction equivalents stabilized by PCET in artificial molecular systems without sacrificial reagents. Our study provides fundamental insight into how light-driven multielectron redox chemistry, for example the reduction of CO_2 or the oxidation of H_2O, can potentially be performed without sacrificial reagents.
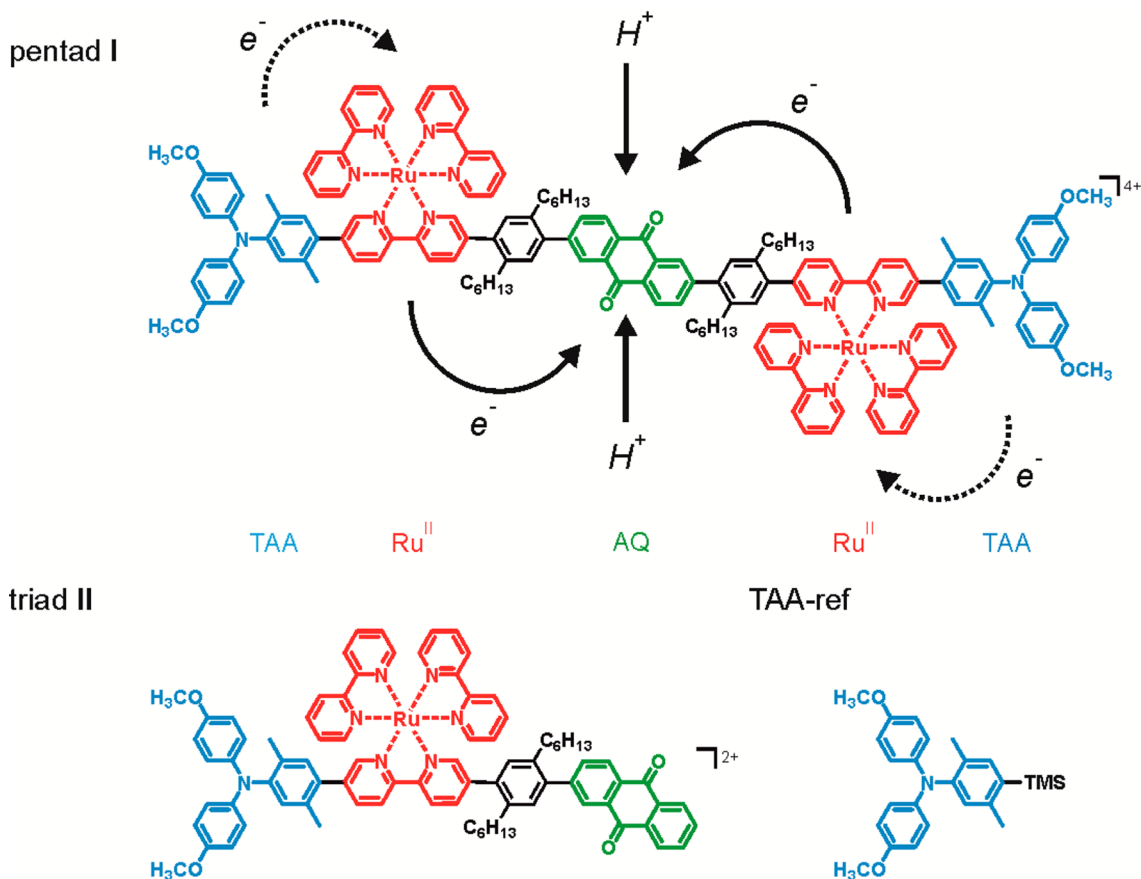
INTRODUCTION

Photoinduced electron transfer in donor−acceptor compounds commonly leads to the formation of electron−hole pairs, and in principle such charge-separated states are interesting for solar energy conversion because they resemble the primary photo-products of photosystem II.[1] However, in natural photosynthesis multiple redox equivalents must be accumulated transiently before they can be used for the actual water oxidation, hydrogen evolution, or CO_2 reduction steps,[2] because these are evidently multielectron redox transformations. Light-driven accumulation of redox equivalents is very tricky to perform in simple artificial systems, because once primary charge-separation has occurred, charge-recombination and other unproductive reactions compete very efficiently with charge accumulation.[3,4] Nature stabilizes the intermediate redox products through proton-coupled electron transfer (PCET),[5] for example in the oxygen-evolving Mn_4Ca complex in which oxidation steps of the Kok cycle are coupled to deprotonation,[2] or in the two-electron reduction of plastoquinone that is coupled to protonation.[6] It seems attractive to exploit PCET for the light-driven accumulation of redox equivalents in artificial donor−acceptor compounds, but until now this has not been accomplished without sacrificial reagents.

When using sacrificial donors or acceptors, light-driven accumulation of redox equivalents is readily achievable because under these conditions the above-mentioned detrimental secondary reactions are largely suppressed.[7−17] However, sustainable solar energy conversion will not be possible with this approach, and hence it is desirable to explore the basic principles of light-driven accumulation of redox equivalents without sacrificial reagents. Currently, there exist only a handful of molecular systems that are able to exhibit light-driven accumulation of redox equivalents under this restriction. Two early systems exhibited very short-lived doubly reduced species ($\tau \leq 5$ ns),[18,19] and a third system relied on the use of TiO_2 nanoparticles.[20,21] A related nanoparticle approach turned out to be useful for multielectron transfer in other systems,[22] and nanoparticle or quantum dot based systems are of course generally promising for accumulation of redox equivalents.[23,24]

Scheme 1. Molecular Structures of Pentad I, Triad II, and TAA-ref[a]

[a]The PCET chemistry expected for pentad I is illustrated.

We recently communicated the first purely molecular system (pentad I, Scheme 1) in which long-lived electron accumulation was possible without sacrificial reagents.[25] Following excitation of the two Ru(II) chromophores, a doubly reduced anthraquinone species (AQ^{2-}) was observable and exhibited a lifetime of 870 ns in neat deaerated CD_3CN at 20 °C.

In this work, we explored pentad I in acetonitrile in the presence of excess *p*-toluenesulfonic acid (TsOH), anticipating that the hydroquinone species (AQH_2) would be accessible under these conditions. Related prior work on single electron transfer with compounds similar to triad II (Scheme 1) provided evidence for the formation of semiquinones ($AQH^{\bullet}$),[26,27] and hence it seemed plausible that AQH_2 could indeed form in pentad I. We were interested to explore whether AQH_2 would form through a concerted or a stepwise PCET mechanism and whether the AQH_2 photoproduct would be even longer lived than the dianion species in neat CD_3CN.[28,29] We find that the light-induced accumulation of reduction equivalents is a stepwise process involving consecutive electron and proton transfer events, but the reverse (thermal) charge-recombination seems to involve a concerted proton-coupled two-electron oxidation of AQH_2. The inverted driving-force effect seems to play a crucial role for the lifetimes of the different doubly reduced photoproducts observed in neat acetonitrile and in the presence of acid.
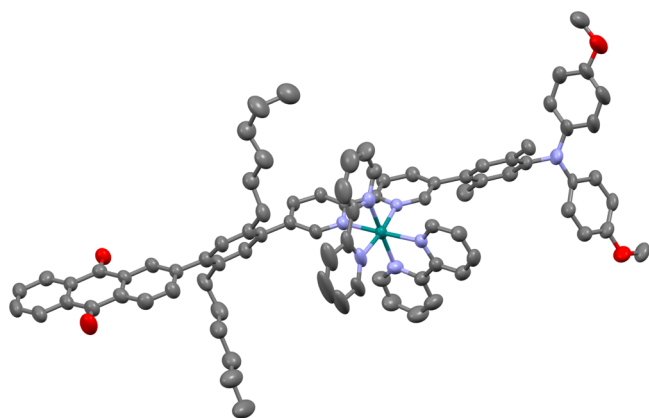
The reduction of AQ in pentad I resembles the reduction of plastoquinone to plastoquinol in natural photosynthesis, in that multiple light-driven electron transfer reactions are coupled to two proton transfer events.[6] Importantly, the overall reaction relies entirely on reversible redox reactions and the input of visible light. The anthraquinone−dihydroxyanthracene redox couple is used for the industrial synthesis of H_2O_2 from molecular oxygen, and consequently it seemed all the more relevant to explore the possibility of reversible two-electron, two-proton-coupled photochemistry in pentad I.
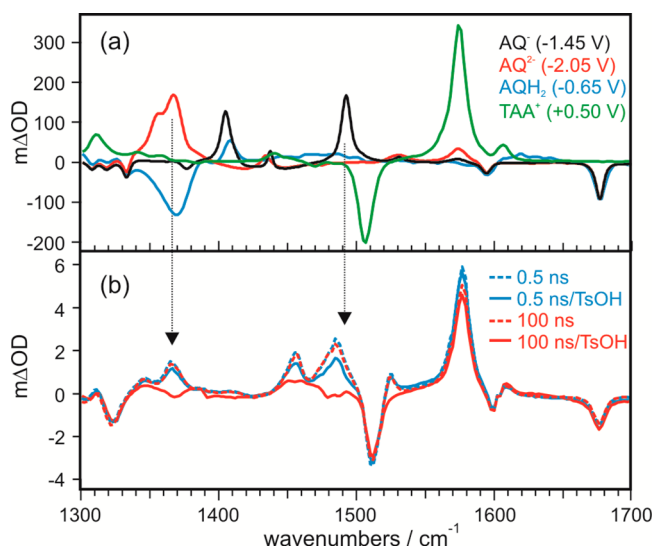
■ RESULTS AND DISCUSSION

In the X-ray crystal structure of triad II (Figure 1), the center-to-center distance between the TAA donor and the AQ acceptor is 22.0 Å. TAA exhibits its common propeller-shaped structure, which is responsible for the relatively low basicity of triarylamines, and this is important for our spectroscopic studies performed in the presence of TsOH. The dihedral angles between the central bpy ligand and its adjacent substituted phenylene bridging units (44.6°, 55.2°) are in the typical range for *p*-xylenes.[30] The structures of one of the methoxyphenyl groups, as well as that of cocrystallized solvent molecules (toluene, $CHCl_3$) are disordered. Crystals of pentad I could not be obtained.

Infrared spectro-electrochemistry of isolated AQ in CD_3CN at 20 °C provided the difference spectra in Figure 2a. The black trace was recorded in neat CD_3CN at a potential of −1.45 V vs $Fc^{+/0}$, and consequently was attributed to AQ^{-}.[31] When a potential of −2.05 V vs $Fc^{+/0}$ was applied, the formation of AQ^{2-} in neat CD_3CN resulted in the red trace. In the presence of 5 equiv TsOH (blue trace), a potential of −0.65 V vs $Fc^{+/0}$ is sufficient to lead to the formation of the $2e^-/2H^+$ reduction product AQH_2 (the semiquinone, $AQH^{\bullet}$, cannot be isolated in

Figure 1. X-ray crystal structure of triad **II** with thermal ellipsoids at the 50% probability level. Hydrogen atoms, counteranions, and solvent molecules have been omitted.

Figure 2. (a) IR difference spectra measured after electrochemical reduction of AQ (5 mM) to AQ$^-$ (black) and AQ^{2-} (red) and oxidation of TAA (5 mM) to TAA$^+$ (using the TAA-ref compound from Scheme 1) in neat CD$_3$CN (green). The difference spectrum of AQH$_2$ (blue) was obtained after electrochemical reduction of AQ in the presence of 5 equiv TsOH in CD$_3$CN. The spectra measured prior to applying any potential served as a baseline. The blue spectrum was scaled to match the change in optical density at 1677 cm^{-1} in the black and red spectra. (b) Comparison of the transient IR spectra of pentad **I** in neat CD$_3$CN (dashed lines) and in the presence of 0.2 M TsOH (solid lines). The spectra were recorded 0.5 ns (blue traces) and 100 ns (red traces) after excitation with 100 fs laser pulses (2 μJ) at 415 nm.

the presence of protons due to potential inversions). Each one of these spectra exhibits bleach signals at 1332, 1594, and 1677 cm^{-1}, originating from the depletion of AQ. Comparison of the two difference spectra recorded in absence of acid in Figure 2a (black and red traces) shows that the most diagnostic feature of AQ^{2-} is an IR absorption at 1366 cm^{-1} (marked by the left arrow in Figure 2), in line with prior reports.[32,33] In contrast, AQH$_2$ lacks similarly strong IR absorptions (blue trace). Aside from a bleach at 1370 cm^{-1} due to the deprotonation of TsOH (Figure S1), the only prominent features in the blue spectrum from Figure 2a is a band at 1407 cm^{-1}, which is attributed to AQH$_2$, but which is much weaker than the 1366 cm^{-1} marker

mode of AQ^{2-}. The IR difference spectrum resulting from oxidation of TAA to TAA$^+$ at a potential of 0.50 V vs Fc$^{+/0}$ in neat CD$_3$CN is shown as a green trace in Figure 2a. The spectrum of TAA$^+$ is mainly composed of a bleach at 1506 cm^{-1} and a signal at 1575 cm^{-1}.

Following excitation of 1 mM pentad **I** in neat CD$_3$CN with a femtosecond laser pulse at 415 nm, the transient IR spectra in Figure 2b were detected, shown here for delay times of 0.5 and 100 ns (blue dotted and red dotted lines, respectively). The comparison to the electrochemically induced difference spectra shown in Figure 2a allows us to assign these spectra. Most importantly, an absorption band at 1366 cm^{-1} is found in the transient spectra, similar to the AQ^{2-} spectrum in Figure 2a (red line), from which we had concluded in ref 25 that AQ^{2-} is indeed formed in pentad **I**. The lack of that band in the triad **II** as well as its quadratic dependence on laser excitation power, indicating two absorbed photons, supported this assignment. We had estimated that under the conditions used to record the data in Figure 2b, 15% of the excited pentad molecules exhibited electron accumulation on AQ to form AQ^{2-}. The remaining 85% underwent only single electron transfer to result in AQ$^-$, the latter of which being identified by a marker mode at 1492 cm^{-1} (see right arrow Figure 2, the spectrum of the reduced pentad **I** shows an additional band at ~1460 cm^{-1} that is not present in AQ$^-$; we assume that this band splits off from the 1492 cm^{-1} band due to the lowering of the symmetry of AQ in the pentad as compared to the isolated AQ). Both singly and doubly reduced states are formed in a few 10s of ps and live for almost 1 μs, hence the transient spectra in absence of TsOH are practically identical after 0.5 and 100 ns (dotted traces in Figure 2b).
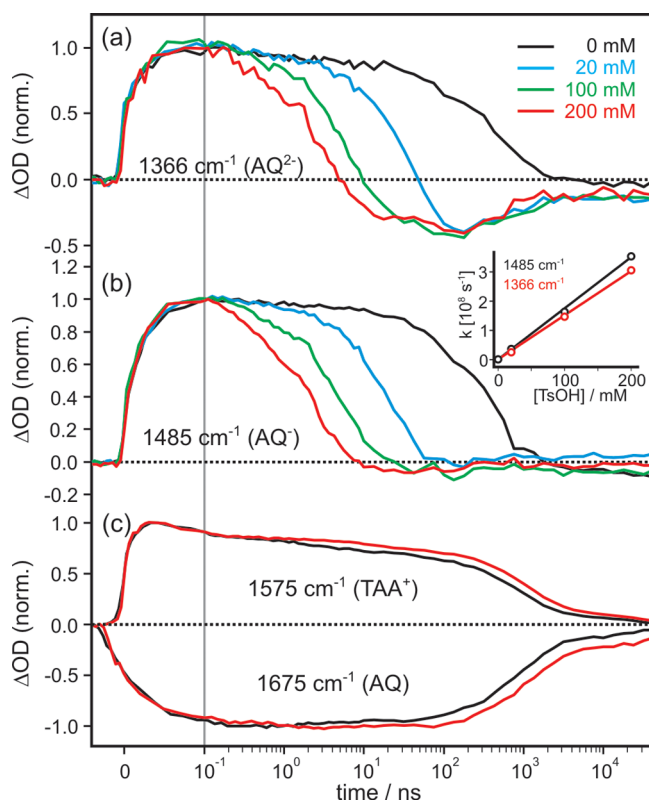
In the presence of 0.2 M TsOH in CD$_3$CN, the transient IR spectra shown in Figure 2b (solid lines) are obtained. After 0.5 ns (blue solid line), the diagnostic absorption bands at 1366 and at 1485 cm^{-1} (slightly shifted from the corresponding band in Figure 2a) are readily detectable, indicating that both AQ^{2-} and AQ$^-$ initially form also under acidic conditions. However, 100 ns after excitation (red solid line) both bands have disappeared while other bands, i.e., the TAA$^+$-related bands at 1575 and at 1510 cm^{-1}, as well as bleach contributions from AQ at 1324, 1598, and 1675 cm^{-1} remain. In the presence of acid, the AQ$^-$ and AQ^{2-} species obviously disappear very rapidly. Because the oxidation product TAA$^+$ persists for much longer and AQ is not yet reoxidized, there must be long-lived reduction products other than AQ$^-$ and AQ^{2-}. It seems plausible that these reduction products are protonated forms thereof. The bleach at 1370 cm^{-1}, reflecting the deprotonation of TsOH, supports that assumption.

Isolated AQH$_2$ only shows an absorption band at 1407 cm^{-1} (blue trace in Figure 2a), which is not detectable in the transient spectra of pentad **I**, presumably because it is a weak band. At the same time, AQH$_2$ can be populated only to maximal 15%.[25] Because the reference spectrum of the semiquinone AQH$^\bullet$ is not accessible due to potential inversions (see comments above), we resort to quantum chemistry calculations performed on the B3LYP/6-311++G(3df,3pd) level of theory with the polarizable continuum model for acetonitrile (see Figure S2).[34] The reliability of these calculations is validated for the AQH$_2$/AQ difference spectrum, which is reproduced essentially quantitatively (compare blue trace in Figure 2a with Figure S2 and keeping in mind that the dominating bleach at 1370 cm^{-1} originates from the deprotonation of TsOH). The AQH$^\bullet$/AQ difference spectrum

(red trace in Figure S2), on the other hand, contains only one significant marker mode at ~1590 cm^{-1}, which likely overlaps with the much stronger band of TAA$^+$. Hence, unfortunately, we are blind to the protonated forms of the reduced anthraquinone by transient IR spectroscopy.

Kinetic traces of the signals related to AQ^{2-} and AQ$^-$ are shown in Figure 3a,b as a function of acid concentration. In
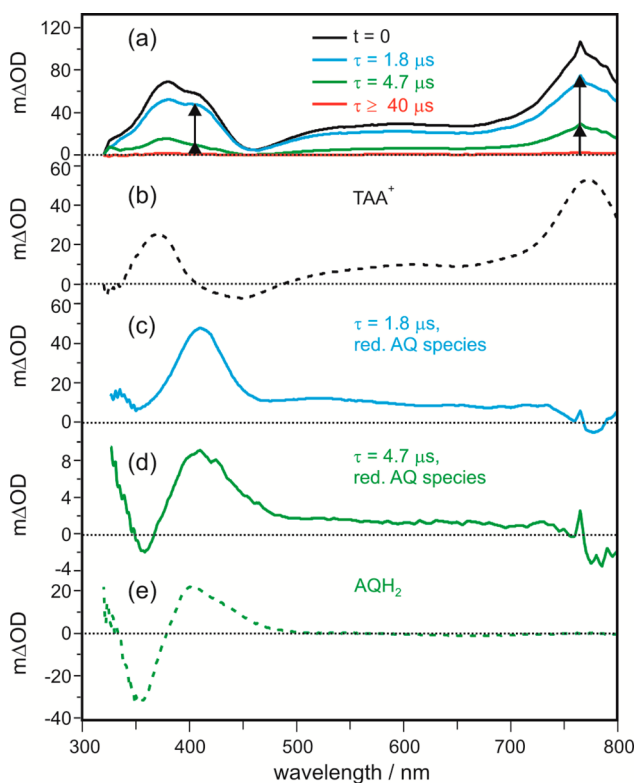

Figure 3. Normalized kinetics of different TRIR absorptions in the presence of increasing TsOH concentrations in CD$_3$CN. The solutions contained 1 mM pentad **I** and were excited at 415 nm with laser pulses of ~100 fs duration (the rise-time of the signal is slower than pulse duration due to the jitter in the synchronization of pump and probe lasers).[25] Detection occurred by monitoring bands related to AQ^{2-} (a) and AQ$^-$ (b). The inset shows the linear dependence of the decay kinetics at 1485 and 1366 cm^{-1} as a function of acid concentration. Panel c shows the normalized kinetics associated with the signal of TAA$^+$ and the ground state bleach of AQ in neat CD$_3$CN (black lines) and in the presence of 200 mM TsOH (red lines). Note that up to 0.1 ns the time scale is linear.

neat deaerated CD$_3$CN, AQ^{2-} and AQ$^-$ decay with lifetimes of 870 and 980 ns (black traces in Figure 3a,b), respectively.[25] In the presence of TsOH, the respective lifetimes shorten considerably (colored traces in Figure 3a,b), and there is a linear relationship between lifetimes and acid concentration (Figure 3b, inset), compatible with the transfer of a single proton. A protonation rate of $(1.5 \pm 0.2) \times 10^9$ M^{-1} s^{-1} can be inferred from the linear fit, indicating a nearly diffusion controlled mechanism.[35] With a single protonation step, both the AQ^{2-} (Figure 3a) and the AQ$^-$ (Figure 3b) marker modes will disappear. A hydroquinone anion species, AQH$^-$, might transiently be formed from AQ^{2-} that then can be protonated a second time. We have no spectroscopic indication for a second protonation step; however, we expect it to happen on the same time scale as the first protonation step. The pK$_a$ of an acid is

related to its deprotonation rate, which may vary over many orders of magnitude, whereas the protonation rate of the conjugated base is diffusion controlled and thus essentially a constant.[36] That is, as long as the second protonation step is thermodynamically possible based on the acidity constants, it will happen on essentially the same time scale as the first protonation step. The pK$_a$ value of TsOH in CH$_3$CN is 8.6.[37] For the reduced AQ species, only pK$_a$ values for aqueous solvent seem to be known, and it is difficult to use these as a basis for estimation of the pK$_a$ values in CH$_3$CN, due to the hydrogen-bonding nature of water. Consequently, we use reported values for 1,4-benzoquinone (BQ) in DMSO to estimate the acidity of the relevant reduced AQ species in acetonitrile.[38] Following a previously published procedure,[37] one obtains pK$_a$(BQH$^-$) = 35.2, pK$_a$ (BQH$_2$) = 29.3, and pK$_a$(BQH$^\bullet$) = 21.5. Assuming a similar pK$_a$ value for AQH$_2$ as for BQH$_2$ (29.3), the second protonation step is thus indeed expected to be exergonic by ~1.2 eV. The kinetic traces at 1443 cm^{-1} (see Figure S3) indicate an additional kinetic process between ~7−50 ns at high acid concentrations. Because that process appears in essentially the same way in both the pentad **I** and the triad **II**, we conclude that it does not reflect the second protonation step. Tentatively, we assign it to a conformational change.

On a microsecond time scale, the AQ-bleach signal as well as the TAA$^+$ signal relax as well, indicating back-electron transfer (Figure 3c). In the presence of protons, that decay is slightly slower. However, the decay occurs in a rather nonexponential manner with a tail extending beyond 40 μs (the upper limit of our setup) that is strongly concentration dependent, indicating a bimolecular charge-recombination that separates reductive and oxidative equivalents on different molecules (Figure S7). Furthermore, we have seen that residual oxygen affects the decay time. We therefore will discuss the charge−recombination in more detail based on transient UV−vis experiments in the following, which can be performed at much lower concentrations (i.e., 20 μM, as compared to 1 mM for the transient IR experiments), and under better deaerated conditions (because no flow-cell is required). We will also see that these UV−vis experiments are complementary to transient IR spectroscopy, as they can indeed identify the hydroquinone (AQH$_2$) and discriminate it from the semi-quinone (AQH$^\bullet$), whereas transient IR spectroscopy has been blind to these two species.

The transient UV−vis data in Figure 4a were obtained by exciting pentad **I** at 532 nm with pulses of ~10 ns duration in deaerated CH$_3$CN containing 0.2 M TsOH. Using such a long laser pulse width, all relevant photoproducts are formed within the duration of the pulses (see above). Transient absorption decays were recorded in 5 nm intervals between 320 and 800 nm, using a detection time window of 40 μs. The resulting decay data (97 transients) were fitted globally to yield species-associated difference spectra (SADS).[39] The best fit was obtained using a biexponential decay function with a very small offset (~1%), the latter reflecting residual signals with decay times longer than 40 μs (related to the remaining bimolecular electron transfer at these low concentrations, see Figure S7). Analogous SADS fits to UV−vis transient absorption data for triad **II** are best fitted with a single-exponential decay function with a very small offset (Figure S8). Exemplary decay data and fits for pentad **I** and the triad **II** are in the Supporting Information (Figure S9).

Figure 4. (a) Transient absorption data from a deaerated CH_3CN solution of 20 μM pentad **I** with 0.2 M TsOH at 20 °C. Excitation was at 532 nm with laser pulses of ~10 ns duration. Black trace: Initial spectrum at $t = 0$. Blue, green, red traces: SADS with the decay times indicated in the inset. The arrows at 407 and 770 nm illustrate that the $\Delta OD_{407}/\Delta OD_{770}$ ratio decreases from 1:1.5 in the blue trace to 1:3.1 in the green trace. (b) Differential absorption spectrum showing the spectral changes associated with oxidation of TAA in pentad **I**, obtained by spectro-electrochemistry in CH_3CN (applied potential: 0.4 V vs $Fc^{+/0}$). (c) Contribution of reduced AQ species to the overall 1.8 μs-SADS, obtained by subtracting the appropriately scaled spectrum from (b) from the blue trace in panel a. (d) Contribution of reduced AQ species to the overall 4.7 μs-SADS, obtained by subtracting the appropriately scaled spectrum from (b) from the green trace in panel a. (e) Differential absorption spectrum for AQH_2 obtained after applying a potential of −1.4 V vs $Fc^{+/0}$ to a solution containing 0.2 mM pentad **I**, 4 mM chloroacetic acid, and 0.1 M $TBAPF_6$ in CH_3CN; the spectrum obtained prior to applying any potential served as a baseline.
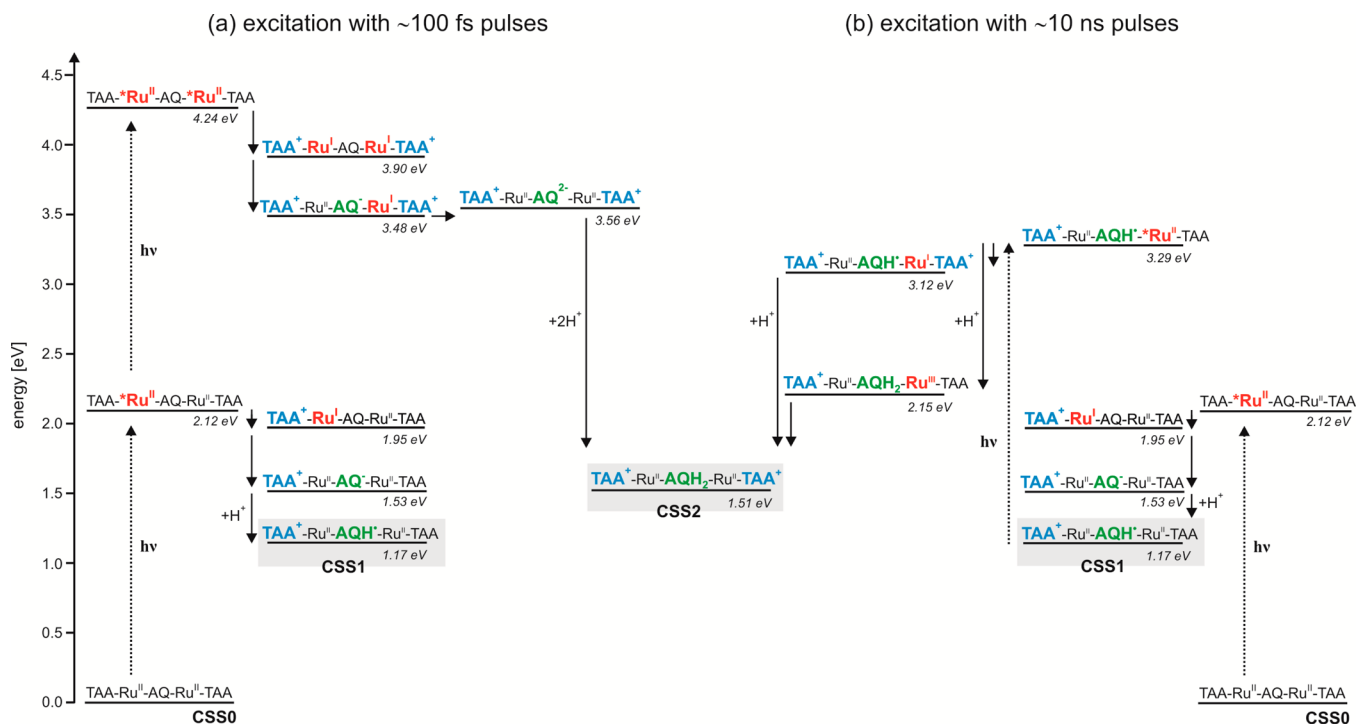
The black trace in Figure 4a represents the spectrum at $t = 0$, which decays with components of 1.8 μs (blue trace) and 4.7 μs (green trace). The transient difference spectra in Figure 4a are essentially linear combinations of the spectra of oxidation and reduction products. The oxidation product is TAA^+ in all cases, as seen readily from prominent absorptions at ~770 nm.[40,41] The difference spectrum of TAA^+ in pentad **I**, obtained by spectro-electrochemistry, is shown in Figure 4b. Reduced anthraquinones do not absorb significantly in the 600−800 nm spectral range,[42,43] and consequently it is possible to scale the TAA^+ difference spectrum from Figure 4b to match the ΔOD values at 770 nm in the individual SADS from Figure 4a, in order to subtract the contribution of TAA^+ to these spectra. What remains are the contributions of the reduced AQ species to the individual SADS, and the resulting spectra are shown in Figure 4c ($\tau = 1.8$ μs) and Figure 4d ($\tau = 4.7$ μs). The spectra in Figure 4c/d are rather similar to one another, and with main

absorption bands between 370 and 480 nm they are both compatible with the formation of either $AQH^{\bullet}$ or AQH_2, i.e., the semiquinone or hydroquinone forms.[28,29] $AQH^{\bullet}$ and AQH_2 have similar extinction coefficients at their absorption maxima in the blue/UV spectral range. Specifically, for $AQH^{\bullet}$ in aqueous isopropanol/acetone mixture, $\varepsilon = 8900$ M^{-1} cm^{-1} at 389 nm,[44] whereas for AQH_2 in ethanol/isopropyl alcohol the extinction coefficient at 382 nm is ~7500 M^{-1} cm^{-1}.[45,46] Going back to the SADS in Figure 4a, we note that the ratio between ΔOD-values at 407 nm (i.e., near the maxima of the reduced AQ species in Figure 4c,d) and the ΔOD values at 770 nm (i.e., at the maximum of the TAA^+ absorption) is significantly different for the 1.8 μs and the 4.7 μs components. Incidentally, TAA^+ does not contribute to the change in absorbance at 407 nm (Figure 4b), and consequently these ratios can be used to estimate the relative quantities of reduced AQ species and TAA^+. From the blue trace in Figure 4a we extract a $\Delta OD_{407}/\Delta OD_{770}$ ratio of 1:1.5, whereas in the green trace the respective ratio is 1:3.1 (see arrows in Figure 4a). Assuming the extinction coefficients of $AQH^{\bullet}$ and AQH_2 at 407 nm are indeed similar as noted above, the differences in $\Delta OD_{407}/\Delta OD_{770}$ ratios can then be explained by attributing the 1.8 μs SADS to a 1:1 mixture of $AQH^{\bullet}$ and TAA^+, and by attributing the 4.7 μs SADS to a 1:2 mixture of AQH_2 and TAA^+. In other words, the 1.8 μs SADS corresponds to an ordinary electron−hole pair which is accessible after absorption of a single photon, whereas the 4.7 μs SADS reflects the charge-accumulated state comprised of a two-electron reduced AQH_2 product combined with two one-electron oxidized species.

UV−vis spectro-electrochemical studies support this interpretation. The difference spectrum in Figure 4e was obtained after applying a potential of −1.4 V vs $Fc^{+/0}$ to a 0.2 mM solution of pentad **I** in deaerated CH_3CN with 4 mM chloroacetic acid. This difference spectrum is in very good agreement with that of the AQ reduction product in Figure 4d. We note that the spectrum of the hydroquinone anion species (AQH^-) exhibits an additional absorption band between 450 and 600 nm,[42] hence it seems clear that the observed species in the 4.7 μs SADS does indeed contain the doubly protonated AQH_2 product rather than AQH^-. This is not surprising because TsOH is present in large excess and it is a much stronger acid than AQH_2, as discussed above.

Based on the relative optical densities of the TAA^+ absorptions at 770 nm in the blue and green traces of Figure 4a, the relative amounts of $AQH^{\bullet}$ and AQH_2 can be estimated. Taking into account that the latter implies the formation of two TAA^+ units, we estimate that under the conditions used here (pulse energy of 15 mJ, $P \approx 1.5$ MW), roughly 15% of all photoexcited pentad molecules undergo double electron transfer to form AQH_2 whereas the remaining 85% form the ordinary $AQH^{\bullet}$ photoproduct resulting from single electron transfer (see Figure S10 for details). This estimate is in agreement with our prior study in neat CD_3CN, where we also estimated a ratio of 15%:85% between AQ^{2-} and AQ^-.[25]

As noted above, all photoproducts in Figure 4a form within the relatively long duration (~10 ns) of the laser pulses used for this experiment, and consequently one merely detects their decay in UV−vis transient absorption. However, the TRIR studies reported above occurred with laser pulses of ~100 fs duration, and this large difference in excitation pulse widths is likely to lead to different reaction pathways for charge accumulation. In the TRIR experiment, both Ru(II) chromophores must be excited initially (Scheme 2, left),

Scheme 2. Energy Level Diagram Established on the Basis of Electrochemical and UV−vis Data for Pentad I[a]

(a) excitation with ~100 fs pulses

(b) excitation with ~10 ns pulses

[a]The main reaction pathways leading to the accumulation of redox equivalents after excitation with ~100 fs pulses (left) and ~10 ns pulses (right) are shown.

followed by electron transfer from TAA to the photoexcited complexes and subsequent reduction of AQ. Although AQ^{2-} forms within 65 ps,[25] the experiments performed in the presence of acid (Figures 2 and 3) show that protonation of AQ^{2-} occurs on a slower time scale (~3 ns at 0.2 M TsOH for the first protonation step), indicating that AQH_2 is formed via a sequence of electron and proton transfer events rather than via concerted PCET. Using the nanosecond pulses, a reaction sequence resembling more the Z-scheme of natural photosynthesis (Scheme 2, right) becomes viable. The formation of TAA^+ and AQ^- requires only 50 ps,[25,47] and protonation of AQ^- occurs with a time constant of ~3 ns (Figure 2). Consequently, when using pulses of ~10 ns duration, absorption of the second photon can occur after the formation of the primary $TAA^+/AQH^\bullet$ photoproduct (called CSS1 in Scheme 2), but ultimately the same final product comprised of two TAA^+ units and one AQH_2 (CSS2) is accessible.

The lifetime of the $TAA^+/AQH^\bullet$ product in deaerated CH_3CN is 1.8 μs (Figure 4a), in line with prior experiments on compounds closely resembling triad II.[27,47,48] The lifetime of the AQH_2 photoproduct under identical conditions is 4.7 μs (Figure 4a), significantly longer than the lifetime of the AQ^{2-} species in neat CD_3CN (870 ns).[25] The energies of the individual states in Scheme 2 were determined based on the redox potentials of pentad I in the presence of 0.2 M TsOH (see Supporting Information for details; Figure S4).

When using deuterated p-toluenesulfonic acid (TsOD), the lifetimes of $AQD^\bullet$ and AQD_2 are 2.5 and 6.6 μs, respectively, under otherwise identical conditions (Figure S5). Thus, there is an H/D kinetic isotope effect (KIE) of 1.4 ± 0.2 for both recombination processes, compatible with concerted PCET to reform the AQ, TAA, and TsOD starting materials.[49,50] In other words, intramolecular reverse electron transfer from

$AQH^\bullet$ or AQH_2 to TAA^+ occurs in concert with proton transfer to TsO^-. However, so-called proton inventory experiments in which the H/D ratio was systematically varied in order to confirm the involvement of two protons in the case of AQH_2 were inconclusive,[51] due to the relatively weak KIE (Figure S6).

■ SUMMARY AND CONCLUSIONS

The formation of AQ^{2-} after absorption of two photons by the $Ru(bpy)_3^{2+}$ sensitizers has significant driving force (Scheme 2), and consequently there is no benefit from concerted PCET, and the overall process is a sequence of fast electron transfer (65 ps) and slower proton transfer events (~3 ns for the first step) when using excitation pulses of ~100 fs duration. With pulses of ~10 ns duration, AQH_2 is also accessible via excitation of an intermediate with $AQH^\bullet$, because reduction and protonation to the semiquinone occurs with a time constant of ~3 ns. The resulting overall process then resembles the Z-scheme of natural photosynthesis.

Given the large energetic stabilization of the $TAA^+-AQH_2-TAA^+$ photoproduct relative to $TAA^+-AQ^{2-}-TAA^+$ (difference of 2.05 eV, Scheme 2a), the lifetime prolongation from 870 ns in neat deaerated acetonitrile to 4.7 μs in the presence of excess TsOH is rather modest. It seems plausible that the photoproduct in neat CH_3CN benefits from the inverted driving-force effect, because single electron transfer from AQ^{2-} to TAA^+ (to result in the TAA^+-AQ^--TAA state at 1.53 eV) is expected to be exergonic by ~2 eV, and double electron transfer from AQ^{2-} to two TAA^+ units even liberates 3.56 eV (Scheme 2a). For reference, in previously investigated compounds closely related to triad II, charge−recombination between AQ^- and TAA^+ was exergonic by ~1.5 eV and occurred clearly in the inverted region.[52,53] By contrast, in

acidic CH_3CN solution, oxidation of AQH_2 by one TAA^+ liberates only 0.34 eV (see Figure S4 including comments and Table S1), and the proton-coupled (single) oxidation of AQH_2 by TAA^+ (to result in the TAA^+-$AQH^\bullet$-TAA (CSS1) state at 1.17 eV) only releases ∼0.3 eV, whereas proton-coupled (double) oxidation of AQH_2 by two TAA^+ units liberates 1.51 eV (Scheme 2b). Thus, for both kinds of processes (single and double electron transfer) the decay of CSS2 is associated with at least ∼1.7 eV less driving force in the presence of TsOH than in neat CH_3CN. This is in line with recombination processes taking place in the inverted (aprotic solution) and the normal regime (protic solution). This could explain why a state storing ca. 3.5 eV (τ = 870 ns) does not decay far more rapidly than a state storing only ca. 1.5 eV (4.7 μs). Thus, the comparison of aprotic and protic solvent environments provides insight into the decay behavior of electron transfer products that store uncommonly large amounts of energy.

As noted above, TAA^+ is in principle thermodynamically competent to oxidize AQH_2 to AQH_2^+ (ΔG_{ET}^0 = −0.34 eV; Figure S4), but the experimentally determined rate for disappearance of AQH_2 exhibits a significant H/D KIE (1.4 ± 0.2). This observation is compatible with a PCET process, in which AQH_2 is oxidized by TAA^+ and deprotonated by TsO^-, respectively, in a concerted fashion. A sequence of proton and electron transfer steps is improbable because deprotonation of AQH_2 to AQH^- is expected to be endergonic by ∼1.2 eV in the presence of TsO^- in acetonitrile (based on pK_a values for TsOH and 1,4-benzoquinone, as discussed above). In the simplest case, concerted PCET between AQH_2, 1 equiv TAA^+, and 1 equiv TsO^- leads to the semiquinone species ($AQH^\bullet$), i.e., CSS1 at 1.17 eV. However, we note that there is no evidence for repopulation of the TAA^+-$AQH^\bullet$-TAA (CSS1) state from the TAA^+-AQH_2-TAA^+ (CSS2) state, indicating that the latter decays directly to the ground state. This would imply a concerted proton-coupled two-electron oxidation, a highly uncommon process in molecular donor−acceptor compounds.

A key feature of the system considered here is that the accumulation of reduction equivalents on AQ is an entirely reversible process without any sacrificial reagents, demonstrating that light-driven multielectron reactions that are coupled to proton transfer steps are possible in molecular systems devoid of sacrificial donors or acceptors. So far, pentad **I** is a unique example in this context, but the proof of principle is now made.

It is remarkable that a comparatively simple system such as pentad **I** is able to mimic the biologically relevant photodriven conversion of plastoquinone to plastoquinol, which relies on a much more complex enzyme machinery. With its relatively long lifetime (4.7 μs), the dihydroxyanthracene (AQH_2) photoproduct can potentially be used as a temporary storage reservoir of reduction equivalents in order to drive slower secondary redox processes that subsequently lead to more stable reduction products. This would be similar to plastoquinol in photosystem II, which ultimately transfers its reduction equivalents to NAD^+ and CO_2.

■ ASSOCIATED CONTENT

ⓢ Supporting Information

The Supporting Information is available free of charge on the ACS Publications website at DOI: 10.1021/jacs.7b01605.

> Syntheses and experimental methods, additional crystallographic, TRIR, transient UV−vis, and electrochemical data, as well as quantum chemical calculations (PDF)

Crystallographic data for triad **II** (CIF)

■ AUTHOR INFORMATION

Corresponding Authors
*peter.hamm@chem.uzh.ch
*oliver.wenger@unibas.ch

ORCID 🟢
Peter Hamm: 0000-0003-1106-6032
Oliver S. Wenger: 0000-0002-0739-0553

Author Contributions
‡These two authors contributed equally.

Notes
The authors declare no competing financial interest.

■ REFERENCES

(1) Wasielewski, M. R. *Chem. Rev.* **1992**, *92*, 435−461.
(2) Kok, B.; Forbush, B.; McGloin, M. *Photochem. Photobiol.* **1970**, *11*, 457−475.
(3) Hammarström, L. *Acc. Chem. Res.* **2015**, *48*, 840−850.
(4) Kuss-Petermann, M.; Wenger, O. S. *Helv. Chim. Acta* **2017**, *100*, e1600283.
(5) Mayer, J. M.; Rhile, I. J.; Larsen, F. B.; Mader, E. A.; Markle, T. F.; DiPasquale, A. G. *Photosynth. Res.* **2006**, *87*, 3−20.
(6) Saito, K.; Rutherford, A. W.; Ishikita, H. *Proc. Natl. Acad. Sci. U. S. A.* **2013**, *110*, 954−959.
(7) Pellegrin, Y.; Odobel, F. *Coord. Chem. Rev.* **2011**, *255*, 2578−2593.
(8) Bonn, A. G.; Wenger, O. S. *Chimia* **2015**, *69*, 17−21.
(9) Konduri, R.; de Tacconi, N. R.; Rajeshwar, K.; MacDonnell, F. M. *J. Am. Chem. Soc.* **2004**, *126*, 11621−11629.
(10) Konduri, R.; Ye, H. W.; MacDonnell, F. M.; Serroni, S.; Campagna, S.; Rajeshwar, K. *Angew. Chem., Int. Ed.* **2002**, *41*, 3185−3187.
(11) Wouters, K. L.; de Tacconi, N. R.; Konduri, R.; Lezna, R. O.; MacDonnell, F. M. *Photosynth. Res.* **2006**, *87*, 41−55.
(12) Matt, B.; Fize, J.; Moussa, J.; Amouri, H.; Pereira, A.; Artero, V.; Izzet, G.; Proust, A. *Energy Environ. Sci.* **2013**, *6*, 1504−1508.
(13) Elvington, M.; Brewer, K. J. *Inorg. Chem.* **2006**, *45*, 5242−5244.
(14) Manbeck, G. F.; Brewer, K. J. *Coord. Chem. Rev.* **2013**, *257*, 1660−1675.
(15) Molnar, S. M.; Nallas, G.; Bridgewater, J. S.; Brewer, K. J. *J. Am. Chem. Soc.* **1994**, *116*, 5206−5210.
(16) Bonn, A. G.; Wenger, O. S. *Phys. Chem. Chem. Phys.* **2015**, *17*, 24001−24010.
(17) Knör, G.; Vogler, A.; Roffia, S.; Paolucci, F.; Balzani, V. *Chem. Commun.* **1996**, 1643−1644.
(18) O'Neil, M. P.; Niemczyk, M. P.; Svec, W. A.; Gosztola, D.; Gaines, G. L.; Wasielewski, M. R. *Science* **1992**, *257*, 63−65.
(19) Imahori, H.; Hasegawa, M.; Taniguchi, S.; Aoki, M.; Okada, T.; Sakata, Y. *Chem. Lett.* **1998**, *27*, 721−722.
(20) Karlsson, S.; Boixel, J.; Pellegrin, Y.; Blart, E.; Becker, H. C.; Odobel, F.; Hammarström, L. *J. Am. Chem. Soc.* **2010**, *132*, 17977−17979.
(21) Karlsson, S.; Boixel, J.; Pellegrin, Y.; Blart, E.; Becker, H. C.; Odobel, F.; Hammarström, L. *Faraday Discuss.* **2012**, *155*, 233−252.
(22) Young, R. M.; Jensen, S. C.; Edme, K.; Wu, Y. L.; Krzyaniak, M. D.; Vermeulen, N. A.; Dale, E. J.; Stoddart, J. F.; Weiss, E. A.;

Wasielewski, M. R.; Co, D. T. *J. Am. Chem. Soc.* **2016**, *138*, 6163−6170.

(23) Valdez, C. N.; Schimpf, A. M.; Gamelin, D. R.; Mayer, J. M. *J. Am. Chem. Soc.* **2016**, *138*, 1377−1385.

(24) Chen, J. Q.; Wu, K. F.; Rudshteyn, B.; Jia, Y. Y.; Ding, W. D.; Xie, Z. X.; Batista, V. S.; Lian, T. Q. *J. Am. Chem. Soc.* **2016**, *138*, 884−892.

(25) Orazietti, M.; Kuss-Petermann, M.; Hamm, P.; Wenger, O. S. *Angew. Chem., Int. Ed.* **2016**, *55*, 9407−9410.

(26) Hankache, J.; Niemi, M.; Lemmetyinen, H.; Wenger, O. S. *J. Phys. Chem. A* **2012**, *116*, 8159−8168.

(27) Hankache, J.; Wenger, O. S. *Chem. - Eur. J.* **2012**, *18*, 6443−6447.

(28) Mayer, J. M. *Annu. Rev. Phys. Chem.* **2004**, *55*, 363−390.

(29) Weinberg, D. R.; Gagliardi, C. J.; Hull, J. F.; Murphy, C. F.; Kent, C. A.; Westlake, B. C.; Paul, A.; Ess, D. H.; McCafferty, D. G.; Meyer, T. J. *Chem. Rev.* **2012**, *112*, 4016−4093.

(30) Hanss, D.; Walther, M. E.; Wenger, O. S. *Coord. Chem. Rev.* **2010**, *254*, 2584−2592.

(31) Quan, M.; Sanchez, D.; Wasylkiw, M. F.; Smith, D. K. *J. Am. Chem. Soc.* **2007**, *129*, 12847−12856.

(32) Cheng, W. X.; Jin, B. K.; Huang, P.; Cheng, L. J.; Zhang, S. Y.; Tian, Y. P. *J. Phys. Chem. C* **2013**, *117*, 3940−3948.

(33) Babaei, A.; Brooksby, P. A.; Flood, A.; McQuillan, A. J. *Appl. Spectrosc.* **2000**, *54*, 496−501.

(34) Frisch, M. J.; Trucks, G. W.; Schlegel, H. B.; Scuseria, G. E.; Robb, M. A.; Cheeseman, J. R.; Scalmani, G.; Barone, V.; Petersson, G. A.; Nakatsuji, H.; Li, X.; Caricato, M.; Marenich, A.; Bloino, J.; Janesko, B. G.; Gomperts, R.; Mennucci, B.; Hratchian, H. P.; Ortiz, J. V.; Izmaylov, A. F.; Sonnenberg, J. L.; Williams-Young, D.; Ding, F.; Lipparini, F.; Egidi, F.; Goings, J.; Peng, B.; Petrone, A.; Henderson, T.; Ranasinghe, D.; Zakrzewski, V. G.; Gao, J.; Rega, N.; Zheng, G.; Liang, W.; Hada, M.; Ehara, M.; Toyota, K.; Fukuda, R.; Hasegawa, J.; Ishida, M.; Nakajima, T.; Honda, Y.; Kitao, O.; Nakai, H.; Vreven, T.; Throssell, K.; Montgomery, J. A., Jr.; Peralta, J. E.; Oliaro, F.; Bearpark, M.; Heyd, J. J.; Brothers, E.; Kudin, N.; Staroverov, V. N.; Keith, T.; Kobayashi, R.; Normand, J.; Raghavachari, K.; Rendell, A.; Burant, J. C.; Iyengar, S. S.; Tomasi, J.; Cossi, M.; Millam, J. M.; Klene, M.; Adamo, C.; Cammi, R.; Ochterski, J. W.; Martin, R. L.; Morokuma, K.; Farkas, O.; Foresman, J. B.; Fox, D. J. *Gaussian 09 Revision A.02*; Gaussian, Inc.: Wallingford CT, 2016.

(35) Rosspeintner, A.; Angulo, G.; Vauthey, E. *J. Am. Chem. Soc.* **2014**, *136*, 2026−2032.

(36) Donten, M. L.; Hamm, P. *J. Phys. Chem. Lett.* **2011**, *2*, 1607−1611.

(37) Kütt, A.; Leito, I.; Kaljurand, I.; Soovali, L.; Vlasov, V. M.; Yagupolskii, L. M.; Koppel, I. A. *J. Org. Chem.* **2006**, *71*, 2829−2838.

(38) Warren, J. J.; Tronic, T. A.; Mayer, J. M. *Chem. Rev.* **2010**, *110*, 6961−7001.

(39) van Stokkum, I. H. M.; Larsen, D. S.; van Grondelle, R. *Biochim. Biophys. Acta, Bioenerg.* **2004**, *1657*, 82−104.

(40) Sreenath, K.; Suneesh, C. V.; Gopidas, K. R.; Flowers, R. A. *J. Phys. Chem. A* **2009**, *113*, 6477−6483.

(41) Sreenath, K.; Thomas, T. G.; Gopidas, K. R. *Org. Lett.* **2011**, *13*, 1134−1137.

(42) Babaei, A.; Connor, P. A.; McQuillan, A. J.; Umapathy, S. *J. Chem. Educ.* **1997**, *74*, 1200−1204.

(43) Pal, H.; Mukherjee, T.; Mittal, J. P. *J. Chem. Soc., Faraday Trans.* **1994**, *90*, 711−716.

(44) Rath, M. C.; Pal, H.; Mukherjee, T. *Radiat. Phys. Chem.* **1996**, *47*, 221−227.

(45) Tickle, K.; Wilkinson, F. *Trans. Faraday Soc.* **1965**, *61*, 1981−1990.

(46) Hamanoue, K.; Sawada, K.; Yokoyama, K.; Nakayama, T.; Hirase, S.; Teranishi, H. *J. Photochem.* **1986**, *33*, 99−111.

(47) Hankache, J.; Niemi, M.; Lemmetyinen, H.; Wenger, O. S. *Inorg. Chem.* **2012**, *51*, 6333−6344.

(48) Hankache, J.; Wenger, O. S. *Chem. Commun.* **2011**, *47*, 10145−10147.

(49) Sjödin, M.; Styring, S.; Åkermark, B.; Sun, L. C.; Hammarström, L. *J. Am. Chem. Soc.* **2000**, *122*, 3932−3936.

(50) Moore, G. F.; Hambourger, M.; Gervaldo, M.; Poluektov, O. G.; Rajh, T.; Gust, D.; Moore, T. A.; Moore, A. L. *J. Am. Chem. Soc.* **2008**, *130*, 10466−10467.

(51) Matta, M. S.; Vo, D. T. *J. Am. Chem. Soc.* **1986**, *108*, 5316−5318.

(52) Kuss-Petermann, M.; Wenger, O. S. *J. Am. Chem. Soc.* **2016**, *138*, 1349−1358.

(53) Kuss-Petermann, M.; Wenger, O. S. *Angew. Chem., Int. Ed.* **2016**, *55*, 815−819.